Journal of Applied Fluid Mechanics, Vol. 16, No. 12, pp. 2396-2400, 2023.
Available online at www.jafmonline.net, ISSN 1735-3572, EISSN 1735-3645.
https://doi.org/10.47176/jafm.16.12.1992

Freestream Temperature Effects on the Receptivity of Hypersonic Boundary Layer Induced by Finite-Amplitude Pulse Entropy Waves

X. Tang[1,2], D. Chen[2†], L. Liu[2], P. Zhu[1], L. Xin[2] and M. Shi[3]

[1] *School of Materials Science and Engineering, Yantai Nanshan University, Yantai, 265713, China*
[2] *Beijing Spacecrafts, China Academy of Space Technology, Beijing 100094, China*
[3] *School of Civil Engineering, Inner Mongolia University of Science and Technology, Baotou, 014010, China*

†*Corresponding Author Email: chendkk@163.com*

ABSTRACT

The unsteady hypersonic flow under finite amplitude pulse entropy perturbation at different freestream temperatures was calculated by direct numerical simulation. The flow response characteristics under the perturbation of entropy waves in freestreaming are analyzed. The temperature effect of freestreaming is studied based on the sensitivity of the boundary layer caused by pulse entropy perturbation. The results show that the higher freestream temperature promotes the first growth of the above third-order modes after leaving the head region, and strongly inhibits the first attenuation. The influence of the freestream temperature on the evolution of the induced disturbance wave is more significant than that on the development of the main flow disturbance waves. Low freestream temperature can suppress the attenuation of the modes below the second order. As the disturbance wave evolves downstream, the frequency band of the finite frequency disturbance wave gradually narrows, and the frequency band narrows faster when the temperature of freestreaming is low than when the temperature of freestreaming is high.

Article History

Received May 10, 2023
Revised July 30, 2023
Accepted August 7, 2023
Available online October 8, 2023

Keywords:

Freestream temperature effect
pulse entropy wave
Boundary layer receptivity
Disturbance mode
Hypersonic boundary layer

1. INTRODUCTION

The boundary layer transition from laminar flow to turbulent flow significantly increases viscous resistance and heat flow density, which severely limits the aerodynamic performance and thermal protection system (Jewell et al., 2017; Zhou et al., 2017; Zhou et al., 2018). Therefore, accurate prediction of the boundary layer transition position is essential. The transition caused by receptivity has been widely examined by many scholars. Wan et al. (2018) have studied the boundary layer's receptivity to slow acoustic waves and investigated two receptive paths. Low-frequency slow acoustic waves have been found to play a leading role downstream of the flow field. Based on boundary layer instability analysis and wind tunnel transition experiments, Liu et al. (2018) have investigated the receptivity and linear phase characteristics and discussed in depth the experimental study of boundary layer transitions. Wagner et al. (2018) have used a combination method of a slender wedge probe and direct numerical simulation to measure freestream disturbance in a hypersonic wind tunnel. Qin and Wu (2016) have analyzed the receptivity characteristics of the wedge-shaped layer to freestream acoustic disturbance, vortex disturbance, and entropy disturbance. Cerminara and Sandham (2017) have studied the leading edge receptivity of the boundary layer to fast and slow acoustic waves in six different cases with Mach numbers between 3.0 and 7.3. The above research into boundary layer receptivity has mainly focused on the generation of unstable waves after external disturbance sources enter the boundary layer through a certain mechanism, involving interactions between unstable waves and shock waves, as well as disturbance evolution characteristics after interactions. Therefore, many scholars have done research on the characteristics of external disturbance. Stemmer et al. (2017) have used direct numerical simulation to analyze the development process of high-frequency velocity disturbance and the role of the chemical model in the development of disturbance revealed by the unsteady three-dimensional simulation considering chemical equilibrium and nonequilibrium effects.

Chou et al. (2017) have shown the interactions between freestream disturbance and flaring cone model experimentally using controlled laser interference. Maddalon et al. (2015) have studied the transition process of hypersonic vehicles via an experimental method

NOMENCLATURE

α	weighting coefficient	ξ	one direction of the general curvilinear coordinate system
β	weighting coefficient	η	another direction of the general curvilinear coordinate system
γ	specific heat ratio	τ_w	friction stress
ε	amplitude of the pulse entropy wave	t	time
$\mathbf{C}_{f'}$	wall friction coefficient disturbance	T	temperature,
f	dimensionless frequency	T_w	wall temperature
F	inviscid term in the y direction	T_0	freestream temperature
F'	η component of the inviscid flux term	u	velocity along x-axis
F_v	viscous term in the y direction	u_0	freestream velocity
F_v'	η component of the viscous flux term	u'	velocity disturbance along x-axis
L	inviscid term along x-axis	v	velocity along y-axis
L'	ξ component of the inviscid flux term	v'	velocity disturbance in y direction
L_v	viscous term in the x direction	W^+	positive flux term
L_v'	ξ component of the viscous flux term	$W^{+'}$	partial differential approximation of W^+
m_n	weighted coefficient	W^-	negative flux term
Ma_0	freestream Mach number	$W^{-'}$	partial differential approximation of W^-
P	pressure	Δ	grid spacing
p'	pressure disturbance	Δt	time increment
ρ'	density disturbance	ρ_0	freestream density
$\mathbf{Q}$	Jacobian matrix	ρ	density
r	head radius of blunt cone	μ_0	freestream viscous coefficient

and shown that the freestream disturbance property has an important influence on boundary layer transition. Tang et al. (2017) have used the direct numerical simulation to solve the unsteady blunt wedge flow field under the action of freestream finitude amplitude slow acoustic waves and analyzed the receptivity characteristics under different amplitude slow acoustic wave disturbances. Goldstein and Ricco (2018) have studied the leading edge receptivity of supersonic flow fields to freestream noise, wall roughness, and other disturbances, and investigated their influences on transition. Based on the above research, the current research on the characteristics of external disturbance has mainly focused on the pressure, velocity, frequency, amplitude, and other characteristics of disturbance. In addition, there has been much research on the thermal characteristics of disturbances, such as wall temperature conditions. Xian et al. (2015) have studied by numerical calculation the influence of wall temperature on the stability under the action of continuous weak disturbance waves. The stability mechanism is different under different temperatures, which may also directly affect the transition position of the boundary layer. Laderman (1976) experimentally verified the effect of wall temperature on the growth of unstable waves and the transition position. Stetson's (1988) experimental study of hypersonic flow in a blunt cone also shows that the cold wall has a significant effect on the development of boundary layer instability. Duan et al. (2010) studied the wall temperature effect with Ma 5 and found that cold walls can enhance the compression effect and coherence of turbulent structures. Yang and Liu (2017) have used numerical calculation and comparative analysis and found that the influence of wall grid size on wall heat flux decreases gradually with the weakening of streamwise aerodynamic heating. Mack (1975, 1984) has pointed out that changes in boundary layer thickness affects the stability, while different wall temperature conditions makes the layer thickness vary. Also, the wall heat flow is related to the ratio of the wall temperature to the boundary layer temperature. A series of studies on wall temperature effects have systematically revealed the influence of wall temperature on the response, acceptance and stability. It has also revealed that the thermal disturbance of hypersonic flow field affects receptivity characteristics and stability mechanism. Therefore, Miselis et al. (2016) and Huang and Zhong (2014) in recent years have realized that disturbance of the freestream temperature spot (a kind of finite-time entropy disturbance) might influence on the layer receptivity. Therefore, based on the freestream temperature spot induced by a laser, they carried out a study on the receptivity. Interactions between the freestream temperature spot and the bow shock wave have been found to be able to excite the 2nd mode unstable wave more efficiently. The acceptability caused by the temperature point of freestreaming is similar to that caused by the continuous single-frequency entropy wave of freestreaming. The above study well illustrates the boundary layer receptivity mechanism casued by freestream temperature spots. However, it is worth mentioning that in hypersonic flight, the freestream thermal state (such as freestream temperature) and freestream disturbance (such as pressure disturbance, velocity disturbance, and entropy disturbance) often exist at the same time and the freestream thermal state usually reflects a change in freestream temperature. However, it can be seen from the research that only few systematic studies on the receptivity to freestream finite-time disturbance, especially regarding finite amplitude pulse disturbance. According to the research results of wall temperature effects and freestream temperature spot effects on receptivity and stability. The study of the effect of pulse disturbance on the acceptability under

different freestreaming thermal conditions provides a new perspective for revealing the acceptability and stability mechanism.

Thus, the unsteady flow field around the blunt cone under the perturbation of finite amplitude pulse entropy of freestreaming is simulated by using the high-order finite difference method, with the sharp cone at Ma 6 having an attack angle of 0 ° and a half cone angle of 8 ° as the object. The interaction between the freestreaming pulse entropy wave and the hypersonic boundary layer under different freestreaming thermal conditions is studied. The development of disturbance modes is analyzed, and the influence of freestreaming temperature on the generation and evolution of disturbance waves is studied in detail.

2. GOVERNING EQUATIONS AND NUMERICAL METHODS

For the boundary layer receptivity problem, the surface of the blunt cone was considered a curved surface. The N-S equations in *x*-o-*y* were transformed into a general system ξ-o-η for convenient numerical calculation of the flow field. The equations were expressed as:

$$\frac{\partial\left(Q^{-1}U\right)}{\partial t}+\frac{\partial L'}{\partial \xi}+\frac{\partial F'}{\partial \eta}+\frac{\partial L_v'}{\partial \xi}+\frac{\partial F_v'}{\partial \eta}=0 \quad , \tag{1}$$

$$L'=\frac{L_v\xi_x+F\xi_y}{Q} \quad , \tag{2}$$

$$L_v'=\frac{L_v\xi_x+F_v\xi_y}{Q} \quad , \tag{3}$$

$$F'=\frac{L\eta_x+F\eta_y}{Q} \quad , \tag{4}$$

$$F_v'=\frac{L_v\eta_x+F_v\eta_y}{Q} \quad , \tag{5}$$

where Q represents the Jacobian matrix; ξ and η the different directions of the general curvilinear coordinate system, respectively; L' and F' the ξ and η-components of the inviscid flux terms, respectively; L_v' and F_v' the ξ and η-components of the viscous flux terms, respectively; L and F the inviscid terms in the x and y-directions in the Cartesian coordinate system, respectively; and L_v and F_v the viscous terms in the x and y-directions of the coordinate axis in the Cartesian coordinate system, respectively.

To simulate the hypersonic unsteady flow field under the perturbation of finite amplitude pulse entropy and ensure calculation accuracy, the high-order accurate finite difference method based on the 5th-order upwind compact scheme, the 6th-order central scheme and the 3rd-order Runge Kutta scheme is used to solve the N-S equation in a general curvilinear coordinate system. The inviscid term is divided into positive flux term and negative flux term by using Steger warming vector flux splitting method (Steger & Warming 1981), and the inviscid term is discretization by using the 5th-order upwind WENO scheme (Liu et al., 1994). Meanwhile, the discretization of the viscous term is carried out using a 6th-order central difference scheme (Zhang et al., 2008), and the time progression is carried out using the 3rd-order TVD Runge Kutta method (Jiang & Shu 1996). At the same time, to avoid the influence on internal point accuracy, the 6th-order single-sided difference method was used at the computational boundary. The above N-S equations were solved by the finite difference method based on Fortran code. This solution method has been successfully applied in our previous work to simulate the sensitivity and stability problems of similar boundary layers (Tang et al., 2014, 2017, 2020). The effectiveness of numerical methods and grid independence verification has been presented in the author's previous paper (Tang et al., 2020), thus this study will not repeat these parts. The spatiotemporal discretization format is as follows:

The inviscid flux was divided into positive and negative flux terms. The 5th-order upwind discrete scheme of inviscid positive flux terms was expressed as

$$W^{+}{}'=\frac{1}{\Delta}(m_1W_{j+3}^{+}+m_2W_{j+2}^{+}+m_3W_{j+1}^{+}+m_4W_{j}^{+}+m_5W_{j-1}^{+}) \quad . \tag{6}$$

The 5th-order upwind discrete scheme of inviscid negative flux term was expressed as

$$W^{-}{}'=\frac{1}{\Delta}(m_1W_{j+4}^{-}+m_2W_{j+3}^{-}+m_3W_{j+2}^{-}+m_4W_{j+1}^{-}+m_5W_{j}^{-}) \quad . \tag{7}$$

In the formulas, the positive flux term is represented by W^{+} and the negative flux term by W^{-}, Δ the grid spacing, $W^{+'}$ and $W^{-'}$ the partial differential approximations of W^{+} and W^{-}, respectively, and m_N the weighted coefficient.

For viscous terms, the 6th-order central difference scheme was expressed as

$$u^{(i)}=\sum_{k=0}^{i=1}\left(\alpha_{ik}u^{(k)}+\Delta t\beta_{ik}L\left(u^{(k)}\right)\right) \quad (i=1,\ 2,\ 3) \quad , \tag{8}$$

where Δt represents the increment of time, $L\left(u^{(k)}\right)$ represents the differential term of $u^{(k)}$ over time, α and β represents different weighting coefficients respectively.

3. MODEL AND CALCULATION CONDITIONS

The Reynolds number was determined by the freestream parameters and the radius of the blunt cone head. This is a dimensionless number used to characterize fluid flow. The value of the Reynolds number was 6000 here, $\mathrm{Re}=\rho_0 r u_0/\mu_0$, where ρ_0 is the freestream density, r the head radius of the blunt cone, u_0 the freestream velocity, and μ_0 the viscosity coefficient. The Mach number of the freestream Ma_0 was 6, cone angle of the calculation model θ at 16°, head radius r at 1 mm, attack angle α at 0°. In the present study, four kinds of freestream thermal states were

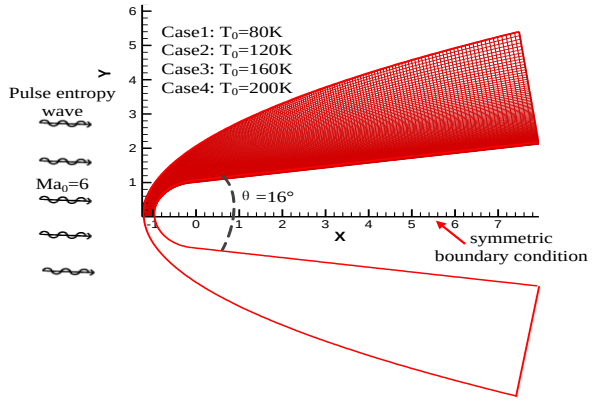

Fig. 1 Numerical model and grid

considered, including freestream temperature T_0 at 80, 120, 160, and 200K. The conditions of no slip and no penetration were adopted on the wall surface of the blunt cone and the wall temperature at T_w at 400K (Fig. 1). Meanwhile, considering the calculation conditions here (Ma at 6 and Re at 6000), the change in γ was tiny and had little impact on the calculation results (Huang & Zhong, 2014; Redford et al., 2012), this study took the specific heat ratio γ to be 1.4. To reduce the amount of calculation, a symmetrical boundary condition was applied to the *x*-axis of the blunt cone model and only the region y >0 calculated. The computational grid in the y >0 region was generated by the local refinement method. The local intensive grid nodes near the blunt cone head and wall were obtained, with the grid number in the y >0 region at 300×120. The grid density here was comparable to that of the literature (Zhang et al., 2008). To facilitate calculation, the freestream parameters and head radius of the blunt cone were used for the dimensionless treatment of the flow field variables.

In the present simulations, the base flow of hypersonic without disturbance under different freestream temperature conditions was first calculated. After the computational flow field remains stable (t=0.0), a half-cycle pulse entropy wave (duration t=2.0) is added to the upstream outer boundary. The expression for the pulse entropy wave is:

$$\begin{bmatrix} u' \\ v' \\ p' \\ \rho' \end{bmatrix} = \begin{bmatrix} 0 \\ 0 \\ 0 \\ \varepsilon Ma_0 \end{bmatrix} e^{i(kx-\frac{F\cdot \mathrm{Re}}{10^6}t)} . \quad (9)$$

In the formula, the velocity disturbance in the freestream direction (*x*-axis direction) is represented by u', velocity disturbance in the freestream orthogonal direction (y-axis direction) by v', pressure disturbance by p', density disturbance by ρ', ε the amplitude of the pulse entropy wave, with the amplitude $\varepsilon = 4\times10^{-2}$. F = 50π, which corresponded to the dimensionless frequency f = 0.25. In the above formula and the following, the superscript "′" indicates the disturbance value of the flow field parameter.

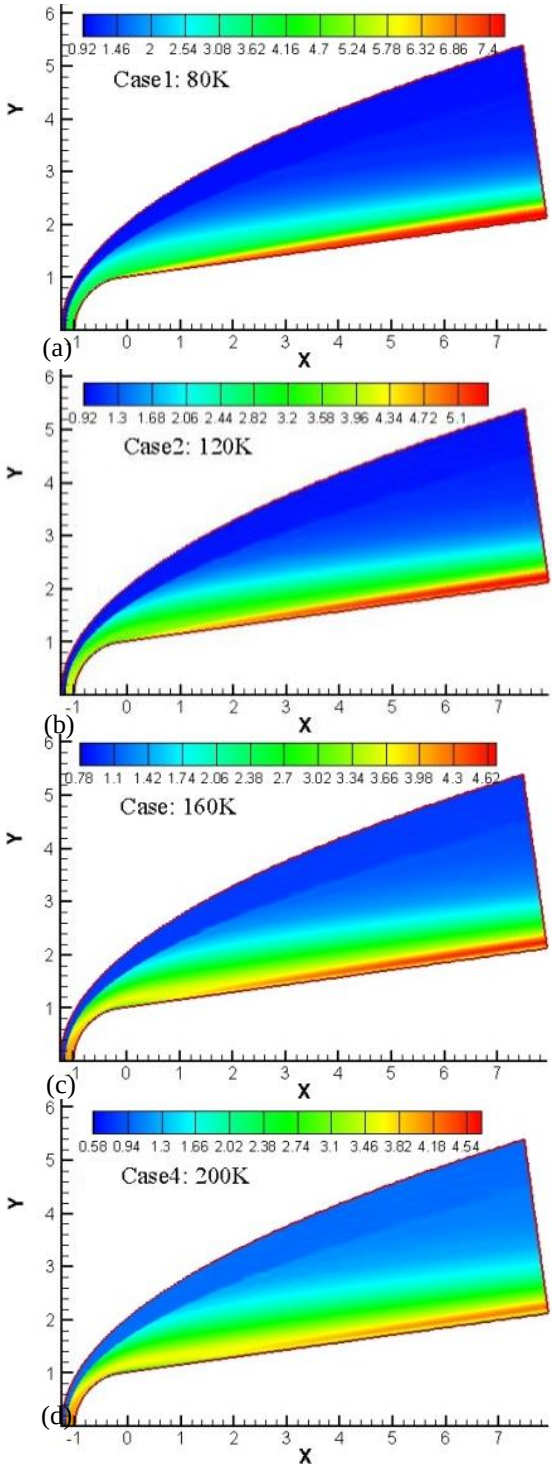

Fig. 2 Contours of steady flow entropy under different freestream temperature conditions

4. DESCRIPTION OF REFERENCE RESULTS AND DISCUSSION

4.1 Analysis of Steady Flow Field

In order to accurately analyze different freestreaming temperature influences on the fixed order hypersonic flow field, the entropy contours of the fixed order hypersonic flow field at 80, 120, 160, and 200 K under the freestreaming temperature T_0 were studied (Fig. 2). It is observed that the distribution of entropy isoline (S) of

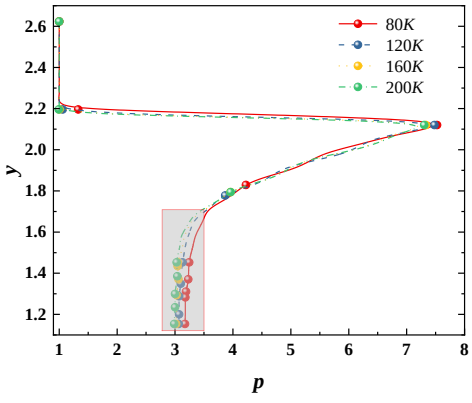

(a)

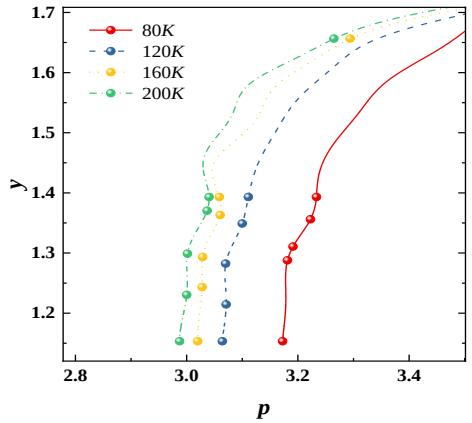

(b)

Fig. 3 Pressure distribution of the wall-normal line at *x* = 1.02073; (b) a locally enlarged view of (a) under different freestream temperature conditions

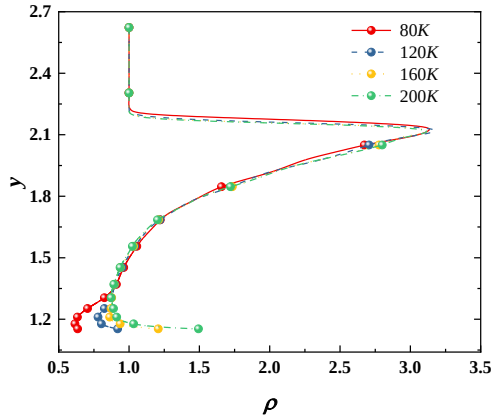

Fig. 4 Density distribution of wall-normal at *x* = 1.02073 under different freestream temperature conditions

the flow field is similar. When the freestreaming temperature increases, the entropy near the wall decreases. According to the relationship between entropy, density, and pressure (Zhou & Cao, 2021; Wan et al., 2023), the entropy distribution is directly related to density and pressure ($S \propto p/\rho^{\gamma}$). The pressure distribution of the wall-normal at *x* = 1.02073 showed that along the average direction of the wall, the pressure in the entropy layer near the wall in the hypersonic flow field decreased significantly with increased freestream temperature (Fig. 3). Huang and Zhong (2011) has studied boundary layer receptivity for blunt compression cells. He found that the response of the flow field after the shock wave to hot spot perturbation also first exhibits a pressure drop phenomenon, although there is a periodic phenomenon of pressure "increase decrease" near the wall afterward. The front part of hotspot pressure retention observed here was consistent with the results of this article. At the same time, the pressure and density distribution of the wall-normal at the position *x* = 1.02073 was examined. Along the average direction of the wall, the density in the entropy layer in the hypersonic flow field was seen to increase significantly with increased T_0 and the above changes not clear in the area far away from the wall (Fig. 4). According to the above equation of entropy, density, and pressure, the entropy value in the hypersonic flow field generally was seen to decrease with increased T_0 without considering the small change of specific heat ratio. Also, the entropy change was more significant near the wall. A similar phenomenon of the pressure and density in the entropy layer near the wall changing violently has been reported in the literature (Balakumar, 2015; Varma & Zhong, 2020). At the same time, the entropy value increased along the flow direction in the downstream area behind the head (Fig. 2), and the entropy value in the downstream area near the wall entropy layer higher. This was due to the combined effect of viscosity and heat conduction near the wall during the compression-expansion process of the flow after passing through the shock wave. This phenomenon was consistent with results obtained by Kara et al. (2008), and Varma and Zhong (2020), who used the direct numerical simulation method to analyze boundary layer flow.

The velocity contours in the *x*-axis of the steady flow field under different freestream temperature conditions were examined (Fig. 5). Although T_0 was changed, the velocity distribution characteristics in the *x*-direction did not change significantly. There were slight differences in speed to further analyze the velocity distribution in detail. The velocity distribution curve in *x* direction of wall-normal at position *x*=1.02073 showed that the temperature of free incoming flow had a slight impact on the velocity distribution and shock layers (Fig. 6). In contrast, the velocity distribution between the boundary and shock layers was not affected by the incoming free flow temperature. Overall, the free-flow temperature affects little on the distribution characteristics of velocity in hypersonic flow fields.

Meanwhile, the change in T_0 changed the thickness of the boundary layer (Figs. 5 and 6). The lower the freestreaming temperature, the thicker the layer. Firstly, reseaches pointed out that wall temperature significantly changes the thickness (Liang et al., 2010; Redford et al., 2012). The thickness under the cold-wall condition is larger than the insulation wall condition. With the isothermal cooling wall condition adopted in this study and under this wall temperature condition, when compared with the adiabatic wall condition, it clearly had a "thickening effect". Under different free-flow temperature conditions, this "thickening effect" would also be significantly different. Second, the flow temperature increased when the free incoming flow

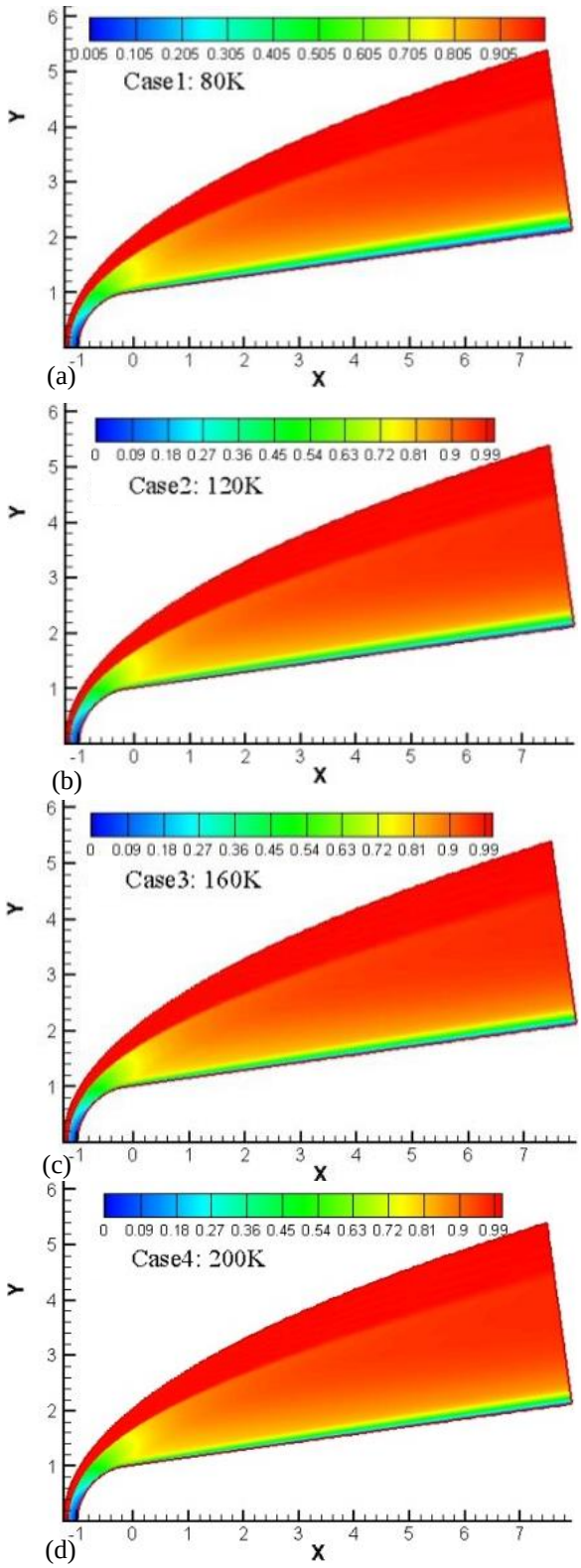

Fig. 5 Velocity contours in *x*-direction of steady flow field under different freestream temperature conditions

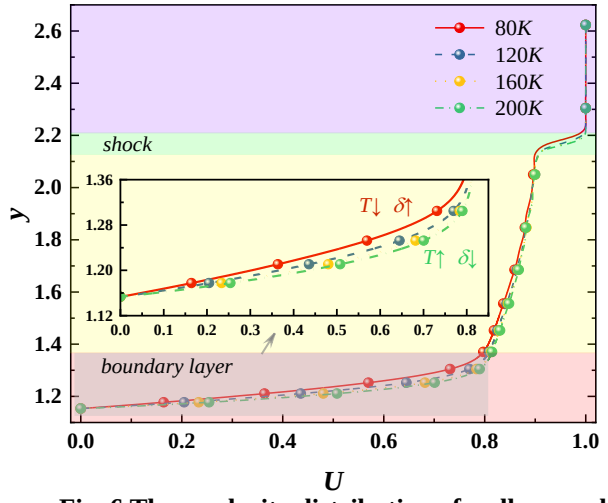

Fig. 6 The *x*-velocity distribution of wall-normal at *x* = 1.02073 under different freestream temperature conditions

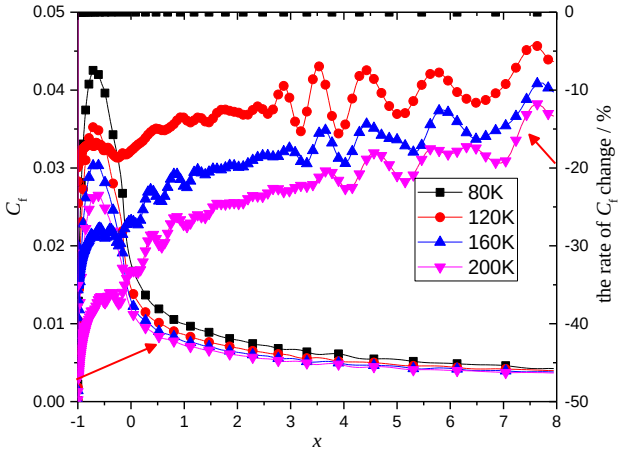

Fig. 7 Distribution and change rate of wall friction coefficient in steady flow under different freestream temperature conditions

passed through the shock wave. After entering the boundary layer, due to the "viscous effect", the thickness of the boundary layer increased. The thickness in this study was seen to be at least determined by the "thickening effect" of the cold wall and "viscous effect". The author tended to maintain that, under the isothermal wall conditions considered here, the influence of the "thickening effect" of the cold wall was stronger than that of the "viscous effect". At a lower T_0, the "thickening effect" of the cold wall would be more significant. Therefore, there was an increase in boundary layer thickness with decreased T_0.

Make (1975, 1984) showed that the change in layer thickness affects its stability. Therefore, the boundary layer shows different stability under different freestreaming temperature conditions.

The distribution of the wall friction coefficient C_f streamwise and the change rate curve of C_f under different T_0 showed that C_f presented different distribution characteristics (Fig. 7). It is observed that, (1) the higher the T_0 was, the smaller the C_f. The wall friction coefficient effectively characterized the shear flow state, and its definition formula was $C_f = \tau_w / \left(\frac{1}{2}\rho U_\infty^2\right)$, where τ_w represents friction stress, which is positively correlated with the velocity gradient

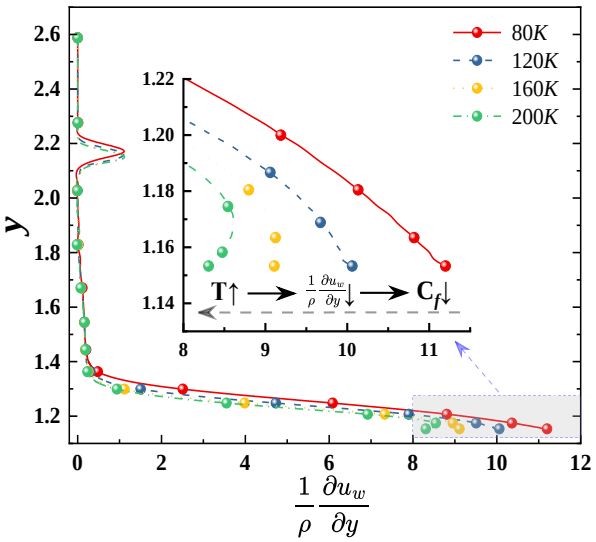

Fig. 8 Normal distribution of wall surface at *x* = 1.02073 under different freestream temperature conditions

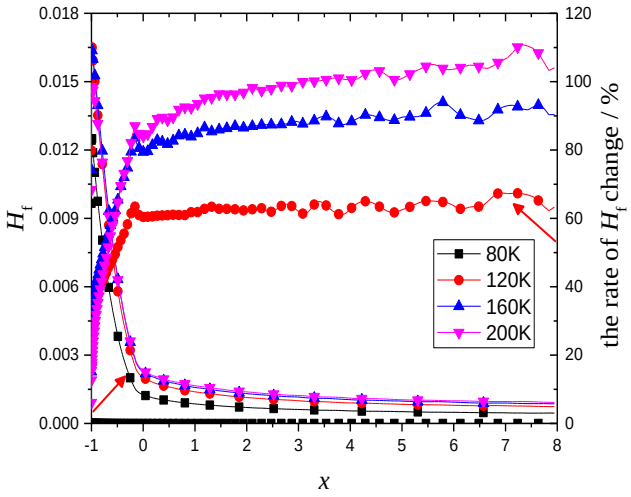

Fig. 9 Distribution and change rate of wall heat flux of steady flow field under different freestream temperature conditions

$\partial u_w/\partial y$, that is, C_f is positively correlated with $\frac{1}{\rho}\frac{\partial u_w}{\partial y}$. The distribution pattern along the average direction of the wall $\frac{1}{\rho}\frac{\partial u_w}{\partial y}$ showed that, as the T_0 increased, $\frac{1}{\rho}\frac{\partial u_w}{\partial y}$ decreased, and therefore C_f also decreased (Fig. 8). In other words, the higher the T_0 was, the smaller the C_f. (2) In the sphere head region, the friction coefficient is more sensitive to the temperature change of freestreaming. At these four T_0, when $-1 < x < 0.5$, C_f increases significantly. C_f reaches its maximum value around $x = -0.5$. When $x > 0.5$, C_f significantly decreases. (3) The difference in C_f under different T_0 decrease along the flow direction. In general, C_f decreases with the increase of T_0, which is due to the decrease of the viscosity coefficient. (4) The right ordinate curve is the change rate of C_f along the flow direction under different T_0 relative to T_0=80K (Fig. 4). We found that high T_0 promoted the change rate of C_f. The change rate of C_f in the sphere head area is more significant than that in the non-head area, with a maximum change rate of -50%.

The distribution of wall heat flux streamwise and the change rate curve of H_f under different T_0 (Fig. 9) showed that (1) the distribution differences of the wall heat flux under the T_0 = 120, 160, and 200K were very small and the wall heat flux under T_0 = 120, 160, and 200K significantly higher than that under T_0 = 80K. (2) Under the four freestream temperature conditions, the wall heat flux presented a trend of continuous attenuation streamwise, with the attenuation significant in the head area. (3) The vertical coordinate curve on the right side showed the change of heat flux streamwise in the steady flow field under different T_0 (Fig. 5). The change rate streamwise was found to increase with increased T_0, that is, the change rate of the heat flux in the head area increased significantly and the change rate of H_f tended to increase slowly after the connection point of the curvature (x = 0).

4.2 Response Analysis of Flow Field to Disturbance Waves

In the *x*-direction velocity perturbation profile at different times (t=3.0, 5.0, 7.0, 9.0), when the freestream temperature is T_0=80K, the velocity near the bow shock wave and the velocity near the wall of the hypersonic blunt cone flow field have relatively significant differences (Fig. 10). The absolute value of velocity disturbance in the *x*-direction of the downstream flow field decreases with the disturbance trend, but the relative velocity disturbance increases. Meanwhile, the boundary layer is a typical viscous compressible flow. The boundary layer is in a strong shear flow state, and the instability is usually in a strong shear flow state. The free flow disturbance enters the flow field through the shock wave, and the disturbance wave interacts with the boundary layer to generate a new unstable mode disturbance. In this process, the disturbance wave will change the flow state. In this study, the flow state will inevitably change after the introduction of free flow disturbance. The flow field forms a "drag wave", and forms a "high-speed/low-speed" area. Therefore, the velocity performance mode near the wall boundary layer has changed significantly. The flow velocity is important to characterize the strong shear flow. It shows the "high-speed/low-speed" region formed by the significant changes in the velocity and disturbance value indicates the structural change of the strong shear flow. C_f is proportional to the normal velocity gradient, which can be used to characterize the shear state of the flow structure. For this reason, the distribution of C_f at different times is investigated (Fig. 11). The distribution of C_f along the flow direction shows that the shear state of the flow structure has changed significantly. This also confirms the influence of the change of the pulse entropy perturbation wave on the structure of the strong shear flow. Fedorov et al. (2013) and Huang and Zhong (2011) also found similar phenomena of hypersonic flow field disturbed by free flow in numerical simulation.

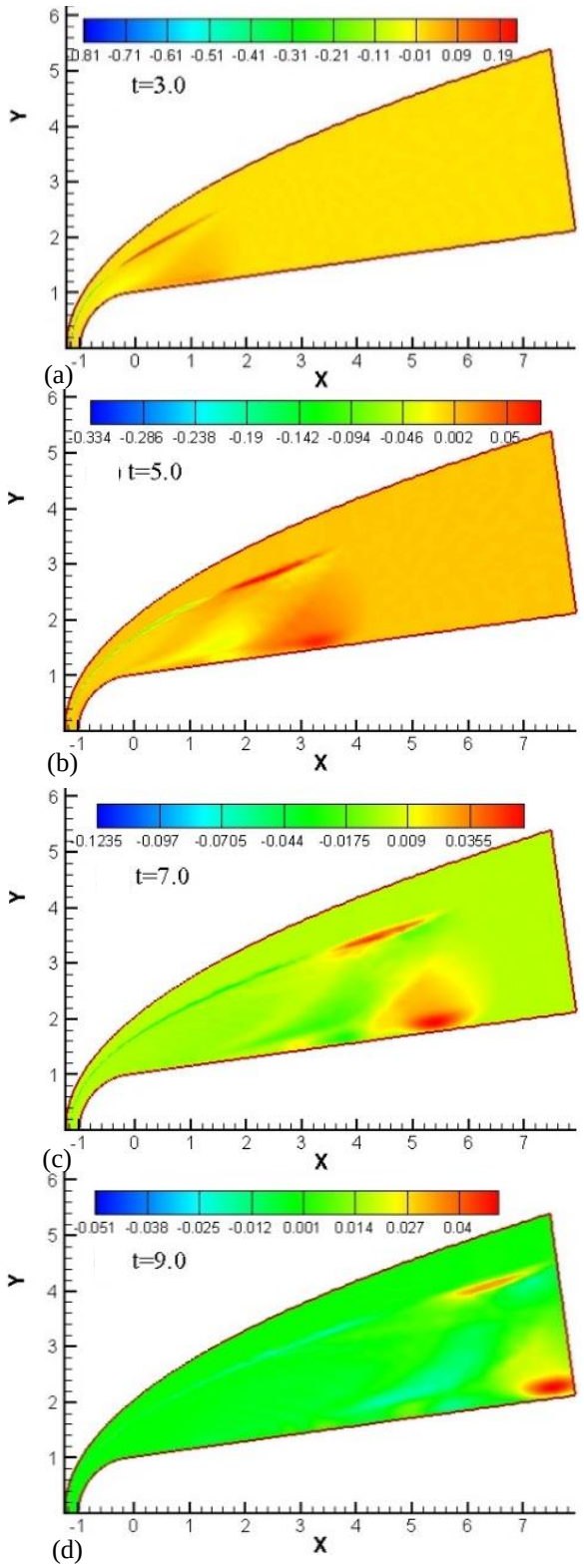

Fig. 10 Contours of velocity disturbance field in *x*-direction of flow field at different times under freestream pulse disturbance (T_0 = 80K)

The contours of flow field entropy disturbances at *t* = 8.0 under different freestream temperature conditions (T_0 = 80, 120, 160, and 200K) and freestream pulse disturbance showed that the changes in T_0 did not significantly change the overall distribution trends of flow field entropy disturbances under limited amplitude pulse disturbance (Fig. 12). There were four or more

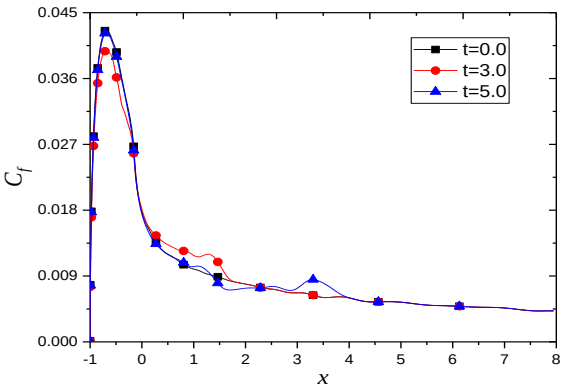

Fig. 11 Distribution of C_f at different times under freestream pulse disturbance (T_0 = 80K)

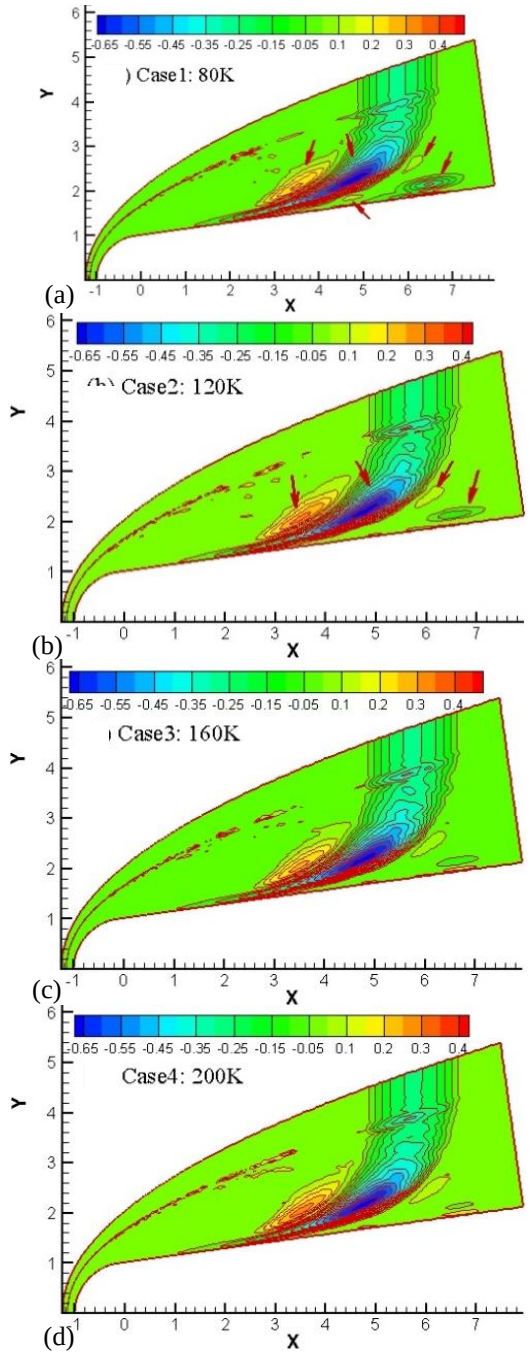

Fig. 12 Contours of flow field entropy disturbance at t = 8.0 under different freestream temperatures and freestream pulse disturbance

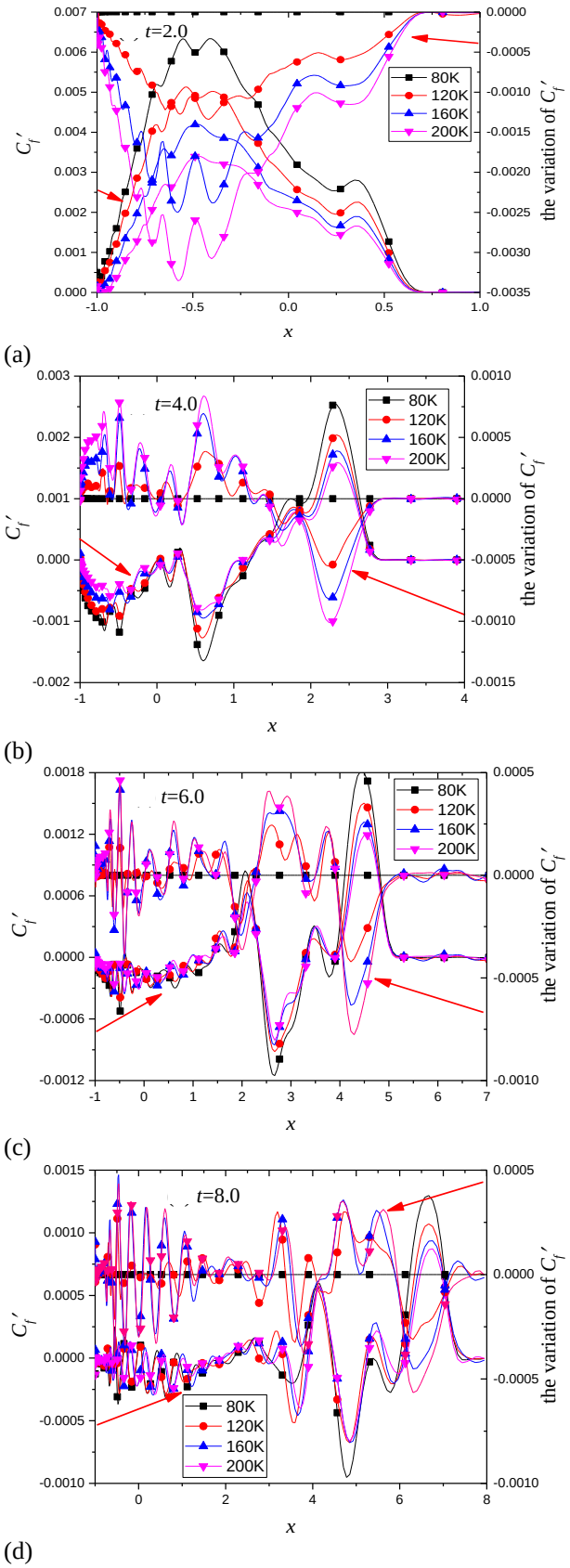

Fig. 13 Comparison of wall friction coefficient disturbance and disturbance variation at different times under different freestream temperatures and freestream pulse disturbance

main disturbance modes in the flow field and a clear boundary between the disturbance modes. The influence of T_0 on the outside was relatively small and on the inside of the boundary layer relatively large. The lower T_0 was, the more complex the disturbance mode near the wall.

A comparison of C_f at different times and the change relative to T_0 = 80K under the freestream finite amplitude entropy disturbance under different T_0 was performed (Fig. 13). (1) Under the freestream finite amplitude entropy disturbance, C_f disturbance decreased with propagation of disturbance waves from upstream to downstream. The higher T_0 was, the smaller the C_f disturbance. (2) When t = 2.0, the C_f disturbance showed an upward trend when x <0.5 and a clear downward trend when x = 0.5, which was caused by the main flow disturbance wave. At this time, the wall was mainly affected by the main flow disturbance wave. (3) With disturbance wave propagation downstream, the main disturbance wave moved backward. The wave near the main disturbance wave was due to the existence of a reflected wave. The residual reflection wave also had a certain influence on C_f. The curve of the right coordinate axis in the figure indicated that the variation of wall friction disturbance at T_0 = 120, 160, and 200K was in an order of magnitude relative to that at 80K and the variation of wall friction disturbance increase with T_0.

The freestream finite amplitude entropy disturbance and the wall heat flow disturbance at different times under different freestream temperature conditions are compared (Fig. 14). The results show that: (1) The response characteristics of wall heat flow disturbance to freestream pulse entropy disturbance are similar to those of C_f disturbance. In other words, under different freestream temperature conditions, the heat flow disturbance value decreases with the downstream propagation of the disturbance wave. (2) In general, the disturbance value of heat flux on the wall under the entropy perturbation of the freestream with finite amplitude increase with T_0. However, there was a clear boundary point (x = -0.75) for the wall heat flux disturbance value curve at different times under different T_0. In a small area (0< x <-0.75) before the boundary point, T_0 has no significant influence on the wall heat flux disturbance value. The lower the T_0 (x >-0.75) after the boundary point was, the greater the wall heat flux disturbance. The reason for this phenomenon was that there was a strong back-and-forth reflection of the disturbance wave at 0< x <0.75.

A comparison of the time-domain curves of pressure disturbance at different locations under different freestream temperatures was performed (Fig. 15). The results show that: (1) The variation trend of the pressure disturbance curve is similar under different freestream temperature conditions. This indicates that before the disturbance amplitude drops to 0.2, the oscillation undergoes a process of increasing and decreasing. At the same time, it was found that the pressure disturbance amplitude near the water head was much greater than that in the area without the water head. In the region of -0.40092<x<7.3338, the lower the T_0, the greater the first peak value. The pressure disturbance appears after the first peak. The higher the T_0 is, the greater the peak value

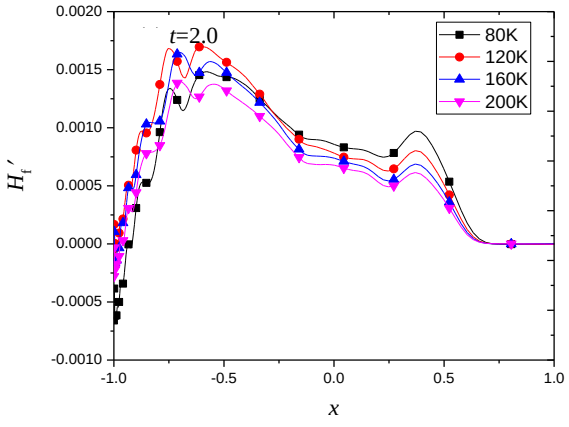

(a)

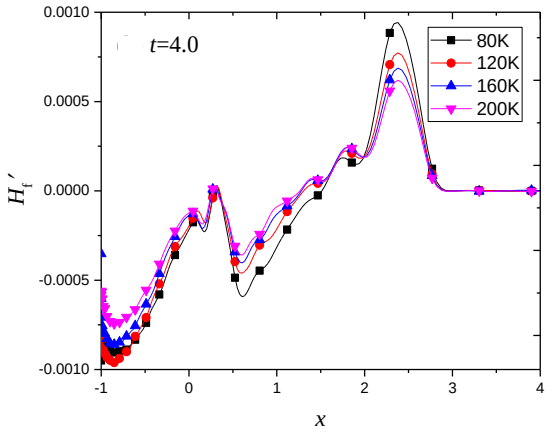

(b)

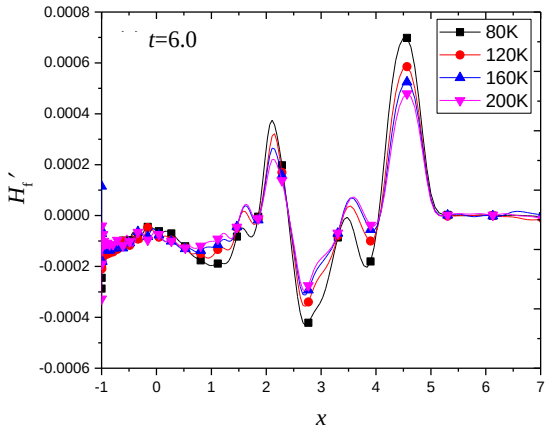

(c)

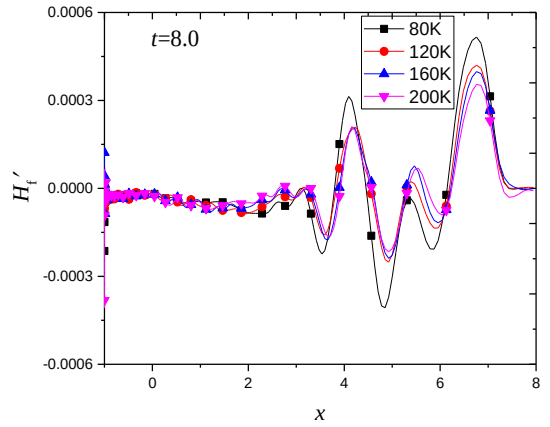

(d)

Fig. 14 Comparison of wall heat flux distribution at different times under different freestream temperatures and freestream pulse disturbance

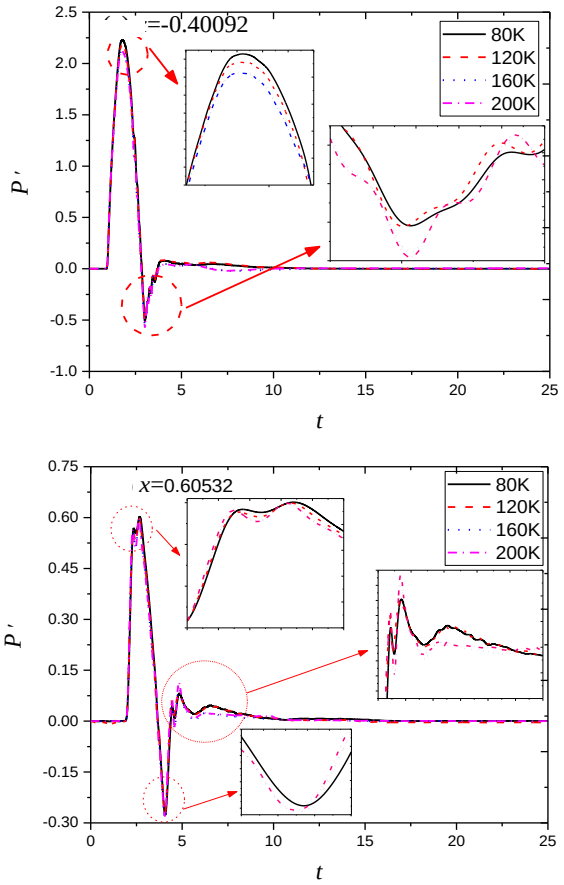

Fig. 15 Comparison of time domain curves of pressure disturbance under different T_0 conditions

is. It is considered that the principal component of the first peak is the main disturbance wave, that is, the low-frequency disturbance wave near the fundamental frequency, the principal component of the pressure disturbance after the first wave is induced by the boundary layer. Therefore, in general, the low T_0 promotes the growth of the main disturbance wave and inhibits the growth of the induced disturbance wave. In addition, the influence of T_0 on the evolution of the boundary layer-induced disturbance wave is relatively greater than that on the main disturbance wave.

The evolution of the f_1 and the 2nd to 6th harmonic frequency (f_2–f_6) modes of the streamwise under different freestream temperatures showed that: (1) In the region of the blunt cone head (-1.0 < x <0.0), the fundamental frequency and amplitude of harmonic modes (f_1–f_6) decreased sharply streamwise (Figs. 16a–16f). Clearly, this was caused by weakening of bow shock intensity from x = -1.0–0.0. After leaving the head region, the amplitude and 2nd-order mode presented a relatively slow attenuation trend and the f_3–f_6 disturbance modes showed a clear increase after leaving the head region. Clearly, the reason for this was that the re-compression effect caused by the blunt cone structure inhibited the attenuation of the f_1 and f_2 disturbance modes and promoted the growth of the f_3–f_6 disturbance modes. As the disturbance wave continued to evolve downstream, most of the disturbance modes began to decay. (2) For the fundamental mode, the lower T_0 was, the larger the amplitude, which showed that the lower T_0 suppressed attenuation. (3) For the 2nd-

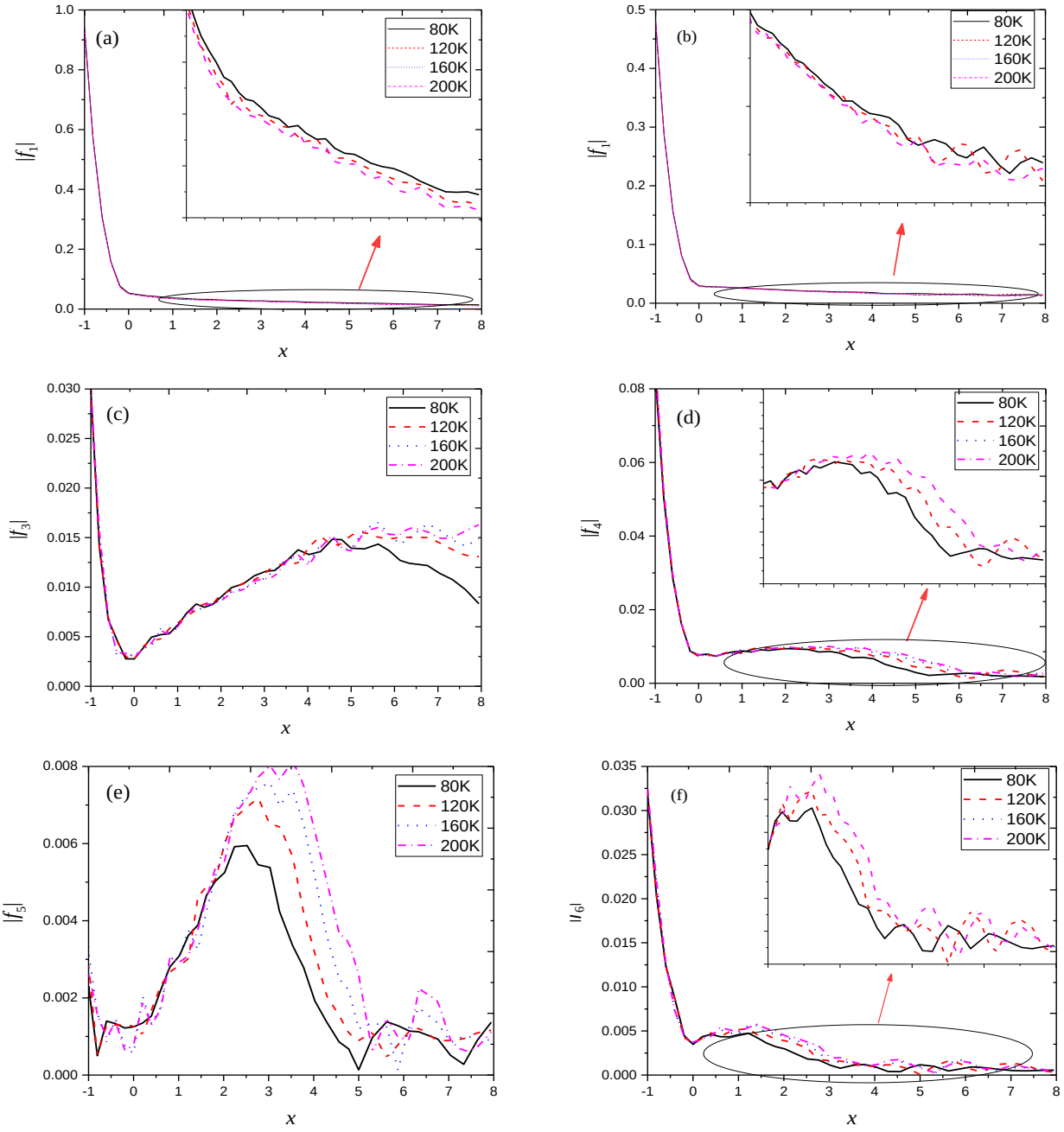

Fig. 16 Evolution trend of Fourier spectrum analysis amplitude along streamwise under different T_0

order mode, when x <5.0, the lower T_0 was, the larger the 2nd-order harmonic mode of the pressure disturbance, which showed that the low T_0 in this area inhibited the attenuation of the 2nd-order harmonic mode. When x >5.0, the T_0 also had a significant impact on the 2nd-order harmonic mode, but there was no clear trend to follow. (4) For the 3rd-order mode, when x<4.0, the amplitude pressure disturbance increase when the T_0 decrease. This indicates that the lower T_0 in this region accelerates the growth of the 2nd-order harmonic modes. When 4.0<x<5.0, the 3rd-order harmonic modal amplitude pressure disturbance begins to decay. When x>5.0, the lower the T_0, the smaller the 3rd-order harmonic modal amplitude pressure disturbance. This shows that the lower T_0 in this region can accelerate the attenuation of the 3rd-order mode. (5) For the 4th-order mode, when 0<x<1.0, the amplitude of the 2nd-order harmonic mode pressure disturbance increase when the T_0 decrease, indicating that the low T_0 accelerates the growth of the 2nd mode. When 1.0<x<6.5, the 4th-order mode amplitude pressure disturbance begins to decay. This shows that the lower T_0 in this region accelerates the attenuation of the 4th-order harmonic mode. When x>6.5, T_0 also has a significant impact on the 4th-order harmonic mode, but there is no obvious change trend. (6) For the 5th-order harmonic mode, the amplitude clearly increased in the region of 0< x <4, which reached a peak value in the region of x = 2.5–3.5 and then rapidly decayed in the region of 3.5< x <5.0. When x >5.0, the 5th-order harmonic mode began to show a complex evolution trend. In the region of 2.5< x <5.0, the later the turning point from growth to attenuation appeared. This showed that high T_0 effectively suppressed 5th harmonic mode attenuation. (7) For the 6th-order harmonic mode, its

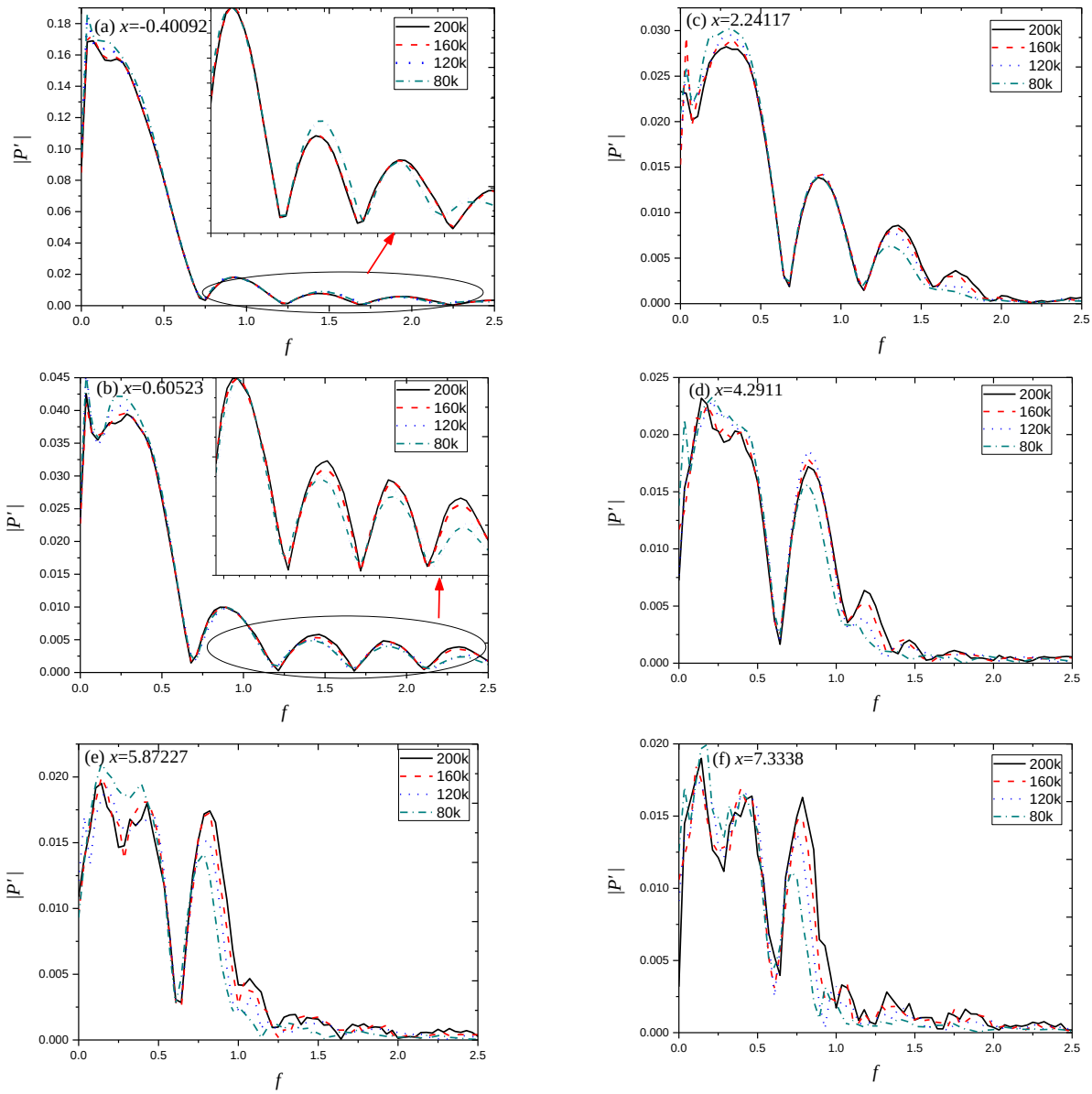

Fig. 17 Amplitude frequency curve under different T_0

evolution trend was similar to the 5th-order. High T_0 effectively restrained the 1st attenuation after leaving the head region. From the above analysis, it was seen that, the lower the T_0 was in the head area and a certain area after the head, the larger the amplitudes and 2nd-order modes of the pressure disturbance were. This showed that lower T_0 suppressed the attenuation of the fundamental and 2nd-order modes. For the 3rd to 6th-order harmonic modes, there was growth after the head area, until a peak (inflection point) which fell into attenuation again. This showed that high T_0 promoted the 1st growth after the head area was out and had a strong inhibitory effect on the 1st attenuation.

The amplitude-frequency curves of six different wall point pressure disturbances, i.e. x = -0.4009, 0.60523, 2.24177, 4.2911, 5.87277, and 7.3338, were examined (Figs. 17a–17f). The distribution and evolution of the disturbance waves were observed to be significantly affected by different freestream temperature conditions under the action of the pulse entropy wave (Fig. 12). (1) Disturbance waves of the finite frequency range were generated under the condition of different freestream flow temperatures. The variation trends of amplitude in the disturbance mode r were similar under different T_0. The variation trends of amplitude in the disturbance mode were similar. The basic frequency disturbance mode near f =0.25 was taken as the main disturbance mode, which was because of the repeated reflection generated after interactions of the inflow disturbance and bow shock between the bow shock and the wall, thus enhancing the amplitude of the disturbance wave (Zhang et al., 2010). (2) In the temperature range considered here, the lower the T_0 was, the larger the basic frequency disturbance mode near f =0.25, no matter the upstream blunt cone head area or the downstream non-head area. This showed that the low T_0 in the head area promoted the development of the low-frequency disturbance mode near f =0.25. (3) After leaving the head region, there were many main disturbance modes, the center frequency of the main disturbance mode group grew with the T_0. Therefore, the high T_0 promoted the

component growth of the high-frequency disturbance wave of $f > f_3$ or f_4. (4) The frequency band of the finite frequency disturbance wave was gradually narrowed with the evolution of downstream, and the frequency band narrowing phenomenon in the case of low T_0 was faster than that in the case of high T_0.

5. CONCLUSIONS

In this study work, the high-order precision finite difference method was used to directly simulate the flow field under the action of finite amplitude pulse entropy perturbation and different freestream temperature conditions. The goal was to analyze effects of different freestream temperatures on the flow field and the response. The influence of T_0 on the generation and evolution of different mode disturbance waves were analyzed through Fourier transform processes. For the steady flow field, the aerodynamic and thermodynamic characteristics of the flow field basically showed similar distribution trends under different freestream temperature conditions. The freestream temperature affect deeply on the steady flow field. Under the action of freestreaming pulse entropy waves, there were four or more major disturbance modes in the flow field under different T_0, with the disturbance modes having clear boundaries. The freestream temperature had a relatively greater impact on the evolution of disturbance waves than it had on the mainstream disturbance wave. High T_0 promoted the 1st growth after leaving the head area and strongly inhibited the 1st attenuation. High freestream temperatures thus promoted the composition of high-frequency disturbance waves with $f > f_3$ or f_4.

ACKNOWLEDGEMENTS

This paper was supported by the National Key R&D Program Young Scientists Project (NO. 2021YFB3400200).

CONFLICT OF INTEREST

The authors declare that there is no known competing financial interests.

AUTHORS CONTRIBUTION

Xiaojun Tang: Methodology, Software, Writing – original draft preparation. Dongkangkang Chen: Methodology, Data curation, Writing – reviewing and editing. Lixia Liu: Conceptualization, Supervision. Pengcheng Zhu: Validation. Resources. Liang Xin: Software, Validation. Mingfang Shi: Investigation, Data curation.

References

Balakumar, P. (2015). *Receptivity of hypersonic boundary layers to acoustic and vortical disturbances*. 45th AIAA Fluid Dynamics Conference.

Cerminara, A., & Sandham, N. D. (2017). Acoustic leading-edge receptivity for supersonic/ hypersonic flows over a blunt wedge. *AIAA Journal*, 55(12), 4234-4244. https://doi.org/10.2514/1.J055749

Chou, A., Balakumar, P., & Schneider, S. P. (2017). Development of instabilities generated by freestream laser perturbations in a hypersonic boundary layer. *AIAA Journal*, 55(3), 799-807. https://doi.org/10.2514/1.J055280

Duan, L., Beekman, I., & Martin, M. P. (2010). Direct numerical simulation of hypersonic turbulent boundary layers. Part 2. Effect of wall temperature. *Journal of Fluid Mechanics*, 655, 419-445. https://doi.org/10.1017/S0022112010000959

Fedorov, A. V., Ryzhov, A. A., Soudakov, V. G., & Utyuzhnikov, S. V. (2013). Receptivity of a high-speed boundary layer to temperature spottiness. *Journal of Fluid Mechanics*, 722, 533-553. https://doi.org/10.1017/jfm.2013.111

Goldstein, M. E., & Ricco, P. (2018). Non-localized boundary layer instabilities resulting from leading edge receptivity at moderate supersonic Mach numbers. *Journal of Fluid Mechanics*, 838, 435-477. https://doi.org/10.1017/jfm.2017.889

Huang, Y., & Zhong, X. (2011). *Numerical study of freestream hot-spot perturbation on boundary-layer receptivity for blunt compression-cones in Mach-6 flow*. 41st AIAA Fluid Dynamics Conference and Exhibit.

Huang, Y., & Zhong, X. (2014). Numerical study of hypersonic boundary-layer receptivity with freestream hotspot perturbations. *AIAA journal*, 52(12), 2652-2672. https://doi.org/10.2514/1.J052657

Jewell, J. S., Parziale, N. J., Leyva, I. A., & Shepherd, J. E. (2017). Effects of shock-tube cleanliness on hypersonic boundary layer transition at high enthalpy. *AIAA Journal*, 55(1), 332-338. https://doi.org/10.2514/1.J054897

Jiang, G. S., & Shu, C. W. (1996). Efficient implementation of weighted ENO schemes. *Journal of Computational Physics*, 126(1), 202-228. https://doi.org/10.1006/jcph.1996.0130

Kara, K., Balakumar, P., & Kandil, O. (2008, June). *Effects of wall cooling on hypersonic boundary layer receptivity over a cone*. 38th Fluid Dynamics Conference and Exhibit.

Laderman, A. J. (1976). New measurements of turbulent shear stresses in hypersonic boundary layers. *AIAA Journal*, 14(9), 1286-1291. https://doi.org/10.2514/3.7217

Liang, X., Li, X., Fu, D., & Ma, Y. (2010). Effects of wall temperature on boundary layer stability over a blunt cone at Mach 7.99. *Computers & Fluids*, 39(2), 359-371.

https://doi.org/10.1016/j.compfluid.2009.09.015

Liu, X. D., Osher, S., & Chan, T. (1994). Weighted essentially non-oscillatory schemes. *Journal of Computational Physics*, 115(1), 200-212. https://doi.org/10.1006/jcph.1994.1187

Liu, X. H.; Lai, G. W.; Wu, J. (2018) Boundary-layer transition experiments in hypersonic flow. *Acta Aerodynamica Sinica*, 36, 196-212, doi: https://doi.org/10.7638/kqdlxxb-2018.0017

Mack, L. M. (1975). Linear stability theory and the problem of supersonic boundary-layer transition. *AIAA Journal*, 13(3), 278-289. https://doi.org/10.2514/3.49693

Mack, L. M. (1984). *Boundary-layer linear stability theory*. California Inst of Tech Pasadena Jet Propulsion Lab.

Maddalon, D. V. & Jr, R. D. W. (2015) Weinstein L M. Influence of measured freestream disturbances on hypersonic boundary-layer transition. *AIAA Journal*, 8(9), 1664-1670, https://doi.org/10.2514/3.5962

Miselis, M., Huang, Y., & Zhong, X. (2016). *Modal Analysis of Receptivity Mechanisms for a Freestream Hot-Spot Perturbation on a Blunt Compression-Cone Boundary Layer*. 46th AIAA Fluid Dynamics Conference .

Qin, F., & Wu, X. (2016). Response and receptivity of the hypersonic boundary layer past a wedge to free-stream acoustic, vortical and entropy disturbances. *Journal of Fluid Mechanics*, 797, 874-915. https://doi.org/10.1017/jfm.2016.287

Redford, J. A., Sandham, N. D., & Roberts, G. T. (2012). Numerical simulations of turbulent spots in supersonic boundary layers: effects of Mach number and wall temperature. *Progress in Aerospace Sciences*, 52, 67-79. https://doi.org/10.1016/j.paerosci.2011.08.002

Steger, J. L., & Warming, R. (1981). Flux vector splitting of the inviscid gas dynamic equations with application to finite-difference methods. *Journal of Computational Physics*, 40(2), 263-293. https://doi.org/10.1016/0021-9991(81)90210-2

Stemmer, C., Birrer, M., & Adams, N. A. (2017). Disturbance development in an obstacle wake in a reacting hypersonic boundary layer. *Journal of Spacecraft and Rockets*, 54(4), 945-960. https://doi.org/10.2514/1.A33708

Stetson, K. F. (1988). On nonlinear aspects of hypersonic boundary-layer stability. *AIAA Journal*, 26(7), 883-885. https://doi.org/10.2514/3.9983

Tang, X., Lv, H., Meng, X., Wang, Z., & Lv, Q. (2014). Stability characteristic of hypersonic flow over a blunt wedge under freestream pulse wave. *Central European Journal of Physics*, 12, 17-31. https://doi.org/10.2478/s11534-014-0421-7

Tang, X., Yu, J., Zhang, H., Li, H., & Shi, M. (2020). Numerical Investigation on the Response Characteristics of Hypersonic Boundary Layer under Different Types of Finite Amplitude Pulse Disturbance Waves. *Journal of Applied Fluid Mechanics*, 14(1), 227-241. https://doi.org/10.47176/jafm.14.01.31485

Tang, X., Zhu, X., Hui, T., Yu, W., Yang, F., & Cao, C. (2017). Receptivity characteristics of a hypersonic boundary layer under freestream slow acoustic wave with different amplitudes. *The European Physical Journal Applied Physics*, 79(3), 31101. https://doi.org/10.2478/s11534-014-0421-7

Varma, A., & Zhong, X. (2020). *Hypersonic Boundary-Layer Receptivity to a Freestream Entropy Pulse with Real-Gas and Nose Bluntness Effects*. AIAA Aviation 2020 Forum.

Wagner, A., Schülein, E., Petervari, R., Hannemann, K., Ali, S. R., Cerminara, A., & Sandham, N. D. (2018). Combined free-stream disturbance measurements and receptivity studies in hypersonic wind tunnels by means of a slender wedge probe and direct numerical simulation. *Journal of Fluid Mechanics*, 842, 495-531. https://doi.org/10.1017/jfm.2018.132

Wan, B., Chen, J., Tu, G., Xiang, X., Yuan, X., & Duan, M. (2023). Effects of nose bluntness on entropy-layer stabilities over cones and wedges. *Acta Mechanica Sinica*, 39(1), 122176. https://doi.org/10.1007/s10409-022-22176-x

Wan, B., Luo, J., & Su, C. (2018). Response of a hypersonic blunt cone boundary layer to slow acoustic waves with assessment of various routes of receptivity. *Applied Mathematics and Mechanics*, 39(11), 1643-1660. https://doi.org/10.1007/s10483-018-2391-6

Xian, L. & Li, X. (2015) Direct numerical simulation on Mach number and wall temperature effects in the turbulent flows of flat-plate boundary layer. Communications in Computational Physics, 17(1), 189-212, https://doi.org/10.4208/cicp.221113.280714a

Yang, J., & Liu, M. (2017). A wall grid scale criterion for hypersonic aerodynamic heating calculation. *Acta Astronautica*, 136, 137-143. https://doi.org/10.1016/j.actaastro.2016.11.043

Zhang, Y., Fu, D., Ma, Y., & Li, X. (2008). Receptivity to free-stream disturbance waves for hypersonic flow over a blunt cone. *Science in China Series G: Physics, Mechanics and Astronomy*, 51(11), 1682-1690. https://doi.org/10.1007/s11433-008-0164-9

Zhou, H.; & Zhang, H. (2017) Two problems in the transition and turbulence for near space hypersonic flying vehicles. *Acta Aerodynamica Sinica*, 35(2), 151-155, https://doi.org/10.7638/kqdlxxb-2017.0016

Zhou, J., & Cao, W. (2021). Effects of entropy layer on the boundary layer over hypersonic blunt cones considering entropy swallowing. *Physics of Fluids*, 33(7). https://doi.org/10.1063/5.0053345

Zhou, L., Zhao, R., & Li, R. (2018). A combined criteria-based method for hypersonic three-dimensional boundary layer transition prediction. *Aerospace Science and Technology*, 73, 105-117. https://doi.org/10.1016/j.ast.2017.12.002